



CHORUS

This is the accepted manuscript made available via CHORUS. The article has been published as:

Topological Defects with Distinct Dipole Configurations in $\text{PbTiO}_3/\text{SrTiO}_3$ Multilayer Films

Lu Lu, Yousra Nahas, Ming Liu, Hongchu Du, Zhijun Jiang, Shengping Ren, Dawei Wang, Lei Jin, Sergei Prokhorenko, Chun-Lin Jia, and Laurent Bellaiche

Phys. Rev. Lett. **120**, 177601 — Published 23 April 2018

DOI: [10.1103/PhysRevLett.120.177601](https://doi.org/10.1103/PhysRevLett.120.177601)

Topological defects with distinct dipole configurations in PbTiO₃/SrTiO₃ multilayer films

Lu Lu,¹ Yousra Nahas,² Ming Liu,¹ Hongchu Du,^{3,4} Zhijun Jiang,^{1,2} Shengping Ren,¹ Dawei Wang,¹ Lei Jin,³ Sergei Prokhorenko,² Chun-Lin Jia^{1,3*} and Laurent Bellaiche^{2†}

¹*The School of Microelectronics and State Key Laboratory for Mechanical Behaviour of Materials, Xi'an Jiaotong University, Xi'an 710049, China*

²*Physics Department and Institute for Nanoscience and Engineering, University of Arkansas, Fayetteville, Arkansas 72701, USA*

³*Ernst Ruska-Center for Microscopy and Spectroscopy with Electrons, Forschungszentrum Jülich GmbH, 52425 Jülich, Germany*

⁴*Central Facility for Electron Microscopy (GFE), RWTH Aachen University, 52074 Aachen, Germany*

Distinct and novel features of nanometric electric topological defects, including dipole waves and dipole disclinations, are presently revealed in the PbTiO₃ layers of PbTiO₃/SrTiO₃ multilayer films by means of quantitative high-resolution scanning transmission electron microscopy. These original dipole configurations are confirmed and explained by atomistic simulations, and have the potential to act as functional elements in future electronics.

Topological structures and defects, which were generally discussed in ordered media in the 1970s [1,2], have currently attracted great attention of researchers in the fields of ferroelectric and magnetic materials [3-13], for which degrees of freedom are electric dipoles and spins, respectively. Therefore the topological structures and defects in these materials typically comprise different types of domain walls (DWs) and other configurations of electric dipoles or magnetic spins [9]. In magnetic materials, besides various traditional domain walls, topological objects such as skyrmions show special configurations with characteristic domain walls based on two types of walls, Bloch- and Néel-type [6]. Being topological objects, magnetic skyrmions are energetically stable on the nanometer scale, thus holding promise for applications in the emerging technology of spintronics [3-5].

In ferroelectrics, physical properties and structures of various DWs have been studied theoretically [14-17] and experimentally [18-23]. It was found that the DWs possess different properties from that of the domains, depending on details of the wall structure [24-26], and thus have been considered as functional elements in future electronics [27]. In addition, theoretical investigations have predicted that nano-size vortex with continuous or sudden rotations of electric dipoles can form in nanostructure of ferroelectric materials due to the large depolarization fields or strains [28,29]. It was also predicted that vortices in a single nanostructure can be switched by a magnetic field without modifying the states of its neighboring nanostructures, and therefore can be used for recording information [28]. In experiments, the continuous rotation of electric dipoles was firstly observed in $\text{Pb}(\text{ZrTi})\text{O}_3$ (PZT) [18] and in BiFeO_3 [19] films. Recently, regular columns of nano-size vortex with continuous rotation of electric dipoles around the column axis were experimentally obtained in the $\text{PbTiO}_3/\text{SrTiO}_3$ (PTO/STO)

superlattice films [8].

In comparison with the recently increasing number of experimental reports on the preparation and characterization of magnetic skyrmions [3-7], there are only limited works in the literature on experimental characterizations of complex and nontrivial configurations of dipoles in ferroelectrics [8,21,30]. In the present study, we report on topological defects with distinct and novel configurations of electric dipoles in epitaxial multilayer films of PTO/STO. Besides nano-scale vortices, we experimentally observe, for the first time, electric dipole waves, dipole disclinations, and other striking electrical topological defects by quantitatively mapping the atomic positions based on atomic-resolution high angle annular dark field (HAADF) images. These topological defects, are reproduced by further simulations that we conduct here.

Figure 1a shows a HAADF image of a multilayer film on the STO substrate viewed along the [100] direction. The image was obtained by adding up 17 original images, which were recorded from the same area of the film in a short time, in order to minimize the effects of random sample drifts and scanning noise (see Supplemental material). The Pb columns appear in the highest contrast (brightest dots), while the Sr and TiO columns show medium and lowest bright contrast, respectively, on a dark background, as shown in the enlarged image (inset). Each film layer has a thickness of about 10 unit cells. The interfaces between the first PTO layer and the STO layer appear sharp with steps of a unit cell scale. Starting from the second period, the interfaces become wavy with many interfacial steps (see Supplemental material Fig. S2).

The atomic positions were determined by means of least squares fitting with two-dimensional Gaussian profiles to the intensity maxima in the image of Fig. 1a [31]. Based on atomic positions, the off-center displacements of the TiO columns were

calculated with respect to the geometric mass center of the surrounding four Pb columns (see Fig. S1). The modulus of the dipole moment is proportional to the off-center displacement [36]. Therefore, the vector map of unit cell dipoles can be derived from the data of the TiO column displacements. Figure 1b shows the vector map of the unit cell dipoles determined on the basis of the off-center displacements of the TiO columns that were measured from the image displayed in Fig. 1a. In comparison with the locations of the PTO and STO layers in Fig. 1a, the dipoles with significant modulus values occur essentially in the PTO layers (yellow areas), as shown by statistical analysis (Fig. S3), which demonstrates the nature of spontaneous polarization in the PTO ferroelectric phase. From Fig. 1b, complex dipole configurations are seen. We also note that a special dipole pattern occurs several times in different regions (denoted by mushroom shapes).

Figures 2a and 2b show the maps of the unit cell dipoles magnified from the areas marked by frames “a” and “b” in Fig. 1b. The PTO film layers are highlighted in yellow color and the STO layers remain white. Figure 2a shows the dipole configurations in the first layer of PTO directly on top of the STO substrate. In the middle part of the map, a nanometric domain can be seen with downward polarization (pink area). In the regions (green) close to the top and bottom interfaces, the local dipoles deviate from the downward direction, forming hyperbola together with the downward oriented dipoles. These dipoles constitute an area with a hyperbola shape, which has been frequently observed in the first PTO layer. In the pink area, the mean value of the off-center displacements for the TiO column peaks was calculated to be about 22 pm, and the corresponding polarization is estimated to be about $70 \mu\text{C}/\text{cm}^2$ (see Supplemental material). On the right of this region the dipoles change directions

continuously as traced by a red curved arrow, forming a vortex with a characteristic of flow-out swirl, where the dipole flux from the center swirls out. On the left of the hyperbola domain, a red ellipse marks a vortex, where the electric dipoles show small in-plane components.

Figure 2b shows another configuration of dipoles, i.e. dipole wave (blue curved arrow) [10]. The dipole vectors adopt directions that significantly deviate from the symmetry-allowed direction [001] of the tetragonal structure, and behave like a fluid that changes direction gradually and continuously (see also Fig. S4). In particular, the feature of the dipole wave shows remarkable resemblance to the result obtained by computations for a very thin PZT film (Fig. 3a in Ref. [10]). Figure 2c further shows that atomistic simulations, which we presently further conduct, can also predict the existence of such striking dipolar waves in PTO films subjected to a compressive strain of -0.6%, corresponding to the one felt by PTO when grown on a STO substrate (see Supplemental material and Ref. [39]). The bound charges of such simulated dipolar waves have been calculated and the resulting distribution of such charges is shown in Fig. S5a. Accompanying the dipole waves, feature of “cylindrical chiral bubbles” can be found located at the region close to the top or the bottom interface/surface, as indicated by a small blue circle in the experimental data of Fig. 2b (see also Fig. S4) and by a red circle in the computational results of Fig. 2c. From the experimental image of Fig. 2b, the unit cells at the centers of the “bubbles” show smaller electrical dipole moment in the (x,y) plane. This likely implies that there is a significant component along the out-of-plane direction. Unfortunately, this component along the out-of-plane direction cannot be experimentally accessed here. On the other hand, simulations have access to such out-of-plane components at the bubbles and do predict that they are rather significant.

Figure 3a shows a magnification of the area marked by frame “c” in Fig. 1b. The thick brown line traces a domain wall separating the top domain with dipoles pointing essentially upward from the bottom domain with dipoles pointing essentially downward. Across the domain wall, the two domains exhibit a tail-to-tail arrangement of the dipoles. In the wall area, the dipoles show evidently the components parallel to the wall plane and pointing from left to right, forming a 90° relation with the upper and lower domains. The domain wall terminates at the point marked by a small red ellipse, where the dipole moments of a few unit cells become close to zero. Around this point, another distinct configuration of dipoles can be recognized (blue area), where the dipoles align essentially along the radius directions and point out, forming a half circle. This configuration is very similar to the 180° disclination that is topologically protected [2], and that has been seen in magnetic systems [40,41] but never observed nor even predicted in ferroelectrics. Figure 3b shows the computational result for PTO film subjected to a compressive strain of -0.6% [42]. The figure provides the in-plane dipolar pattern in a middle layer of the film. The obtained predicted pattern reveals strong similarities with the experimentally observed one (Fig. 3a) and both numerical and experimental results indicate that the system supports a dipolar disclination. The bound charges of the simulated disclination of Fig. 3b have been calculated and their resulting distribution is shown in Fig. S5b. Note that similar configurations have been observed in other parts of Fig. 1b, and that a similar topological defect is shown in Fig. S4 for which the dipoles adopt an opposite direction in comparison with the case of Fig. 3a.

In these atomistic calculations on PTO films under a compressive strain of -0.6%, we find that the dipolar wave (Fig. 2c) numerically obtained through annealing the system, corresponds to the ground state of the system with a total energy per unit

cell of -2.3 mHa with respect to a paraelectric state. While large compressive strain, favoring out-of-plane components of the dipoles, leads to 180 degree domains, with the domain walls separating these up and down domains adopting vortices, when a more moderate strain is rather applied, dipoles acquire in-plane components, thereby transforming the vortices at the domain walls into dipolar waves [10]. Interestingly, we numerically found that the range of strain, for which the dipolar wave is the ground state of PTO, is from -1% to 0%. Moreover, abruptly quenching this same system (PTO films under compressive strain of -0.6%) from high to low temperatures, yields a configuration that hosts the dipolar disclination (Fig. 3b) and that is metastable with a total energy per unit cell of -0.45 mHa with respect to a paraelectric state. The different contributions to the total energy (in mHa/unit cell) for the dipolar disclination (dipolar wave) are 6.4 (9.2), 2.8 (3.9), 2.5 (0.51), -2.3 (-0.3), and -9.9 (-15.6) for on-site, short-range, elastic, electrostrictive and dipole-dipole energies, respectively. One can, e.g., see that what allows both topological defects to be stable (i.e., to have a negative energy with respect to a paraelectric state) and the dipolar waves to be more stable than the disclination are electrostriction and dipole-dipole interactions. Such features are fully consistent with the aforementioned facts that in-plane dipoles want to form under moderate strain (because of electrostriction) and that up and down domains exist in the dipolar waves (because dipole-dipole interactions are known to be related to the screening of the depolarizing field in nanostructures, as e.g.. detailed in Ref. [48]).

Figure 4 shows another vector map of the electric dipoles in the first PTO layer of a different area of the PTO/STO multilayer film. In this map, regular (three) hyperbola domains (pink-green areas) can be clearly seen, which penetrate the whole PTO layer. All these domains have the downward polarization in the main part.

Surprisingly the regions between these hyperbola domains exhibit also essentially downward polarization. However, the amplitude of the polarization is much smaller than those of the neighboring regular domains in pink. We note another distinct feature that, at the center of these regions (small green ellipses), the direction or modulus of the dipoles is significantly different from the surrounding ones. It also bears resemblance with the recently predicted hedgehog/antihedgehog dipolar patterns in the tetragonal phase of ferroelectrics (see Fig. 2 of Ref. [13]).

Recent investigation of dipole configurations in proper ferroelectrics (BaTiO_3) by calculations showed that nontrivial configurations of dipoles could be stabilized by a new mechanism of topological protection, that is finite-temperature fluctuations of local dipoles [13]. It was shown that the finite-temperature fluctuations of local dipoles favor the formation of topological point defects in the tetragonal polar phase and topological line defects in the orthorhombic polar phase. The 1D vortices [8] structures observed in STO/PTO systems on SrRuO_3 -buffered DyScO_3 substrates could be partially related to the contribution of orthorhombic constrain from the substrate and the buffer layer. Differently, in our multilayer systems, we used cubic STO as the substrate, which favors the c-axis-orientated PTO film with tetragonal structure. According to the effects of finite-temperature fluctuations, topological point defects, such as hedgehog- and antihedgehog-like configurations [49], are highly expected in a tetragonal state. Indeed, and as indicated above, the observed dipole configurations (small green ellipses in Fig. 4) can be related to the onset of point defects (e.g., hedgehogs and antihedgehogs), in which dipoles with 3D orientations are expected, due to the relative smaller in-plane modulus of dipoles in comparison with those in the hyperbola domains. The important point of the calculations in Ref. [13], which has strong relation with our experimental

data, is the sufficiently high thermal entropy for the tetragonal and orthorhombic phases, which allows local dipoles to significantly deviate from orientations defined by the crystal symmetry. Our experimental observations indeed show that the configuration of local dipoles can deviate significantly from the [001] direction in the PTO layers. This deviation of local dipoles from a high-symmetry direction was also observed in the R-phase of BiFeO_3 [50].

In conclusion, dipole configurations in the epitaxial STO/PTO multilayer films have been observed. Nano-scale electric dipole waves, dipole disclinations and other distinct configurations are found experimentally for the first time. Further atomistic simulations that we conduct confirm and explain the existence of these dipole configurations. Our observations are expected to stimulate further experimental and theoretical investigations on complex configurations of electric dipoles in ferroelectrics and related properties, which have been discussed theoretically for ordered media [2].

We thank K. Tillmann for reading the manuscript and comments. L.L., M.L., S.R., Z.J., D.W. and C.-L.J. acknowledge the supports by the National Natural Science Foundation of China under Grant No. 51390472, 11574246, and the National Basic Research Program of China (2015CB654903). Y.N. and L.B. acknowledge the ARO grant W911NF-16-1-0227. H.D. acknowledges the support from the Deutsche Forschungsgemeinschaft (DFG) under grant of the SFB 917 Nanoswitches. S.P. thanks the DARPA grant HR0011-15-2-0038 (MATRIX program).

REFERENCES

1. G. Toulouse and M. Kleman, *Journal de Physique Letters* **37**, 149 (1976).
2. N. D. Mermin, *Rev. Mod. Phys.* **51**, 591 (1979).
3. F. Jonietz *et al.*, *Science* **330**, 1648 (2010).
4. T. Schulz *et al.*, *Nature Phys.* **8**, 301 (2012).
5. A. Fert, V. Cros and J. Sampaio, *Nature Nanotech.* **8**, 152 (2013).
6. I. Kézsmárki *et al.*, *Nature Mater.* **14**, 1116 (2015).
7. Z.-A. Li *et al.*, *Nano Lett.* **17**, 1395 (2017).
8. A. K. Yadav *et al.*, *Nature* **530**, 198 (2016).
9. J. Seidel, R. K. Vasudevan and N. Valanoor, *Adv. Electron. Mater.* **2**, 1500292 (2016).
10. D. Sichuga and L. Bellaiche, *Phys. Rev. Lett.* **106**, 196102 (2011).
11. N. Choudhury, L. Walizer, S. Lisenkov and L. Bellaiche, *Nature* **470**, 513 (2011).
12. Y. Nahas *et al.*, *Nature Commun.* **6**, 8542 (2015).
13. S. Prokhorenko, Y. Nahas and L. Bellaiche, *Phys. Rev. Lett.* **118**, 147601 (2017).
14. I. Kornev, H. Fu and L. Bellaiche, *Phys. Rev. Lett.* **93**, 196104 (2004).
15. P. Aguado-Puente and J. Junquera, *Phys. Rev. Lett.* **100**, 177601 (2008).
16. A. Lubk, S. Gemming and N. A. Spaldin, *Phys. Rev. B* **80**, 104110 (2009).
17. W. Ren *et al.*, *Phys. Rev. Lett.* **110**, 187601 (2013).
18. C. L. Jia, K. W. Urban, M. Alexe, D. Hesse and I. Vrejoiu, *Science* **331**, 1420 (2011).
19. C. T. Nelson *et al.*, *Nano Lett.* **11**, 828 (2011).
20. Y. L. Tang *et al.*, *Science* **348**, 547 (2015).
21. J.J.P. Peters, G. Apachitei, R. Beanland, M. Alexe and A. M. Sanchez, *Nature Commun.* **7**, 13484 (2016).

22. X.K. Wei *et al.*, *Nature Commun.* **7**, 12385 (2016).
23. R. K. Vasudevan *et al.*, *ACS Nano* **5**, 879 (2011).
24. J. Seidel *et al.*, *Nature Mater.* **8**, 229 (2009).
25. S.-Y. Yang *et al.*, *Nature Nanotech.* **5**, 143 (2010).
26. N. Balke *et al.*, *Nature Phys.* **8**, 81 (2012).
27. G. Catalan, J. Seidel, R. Ramesh and J. F. Scott, *Rev. Mod. Phys.* **84**, 119 (2012).
28. I. Naumov, L. Bellaiche and H. Fu, *Nature* **432**, 737 (2004).
29. Z. Jiang, B. Xu, F. Li, D. Wang and C. L. Jia, *Phys. Rev. B* **91**, 014105 (2015).
30. A. R. Damodaran *et al.*, *Nat. Mater.* **16**, 1003 (2017).
31. See Supplemental Material for detailed description, which includes Refs. [32-35].
32. H. Du, C.-L. Jia and J. Mayer, *Chem. Mater.* **28**, 650 (2016).
33. C. B. Markwardt, *Non-Linear Least Squares Fitting in IDL with MPFIT*. In *Astronomical Data Analysis Software and Systems XVIII: Proceedings of a Workshop Held at Hotel Loews Le Concorde, Quebec City, QC, Canada, 2-5 November 2008*.
34. J. F. Nye, *Physical Properties of Crystals: Their Representation by Tensors and Matrices*; Clarendon Press; Oxford University Press: New York, 1985.
35. P. L. Galindo *et al.*, *Ultramicroscopy* **107**, 1186 (2007).
36. See Supplemental Material for detailed description, which includes Refs. [37-38].
37. Y. Kuroiwa *et al.* *Phys. Rev. Lett.* **87**, 217601 (2001).
38. G. Sághi-Szabó, R. E. Cohen and H. Krakauer, *Phys. Rev. Lett.* **80**, 4321 (1998).
39. Z. Jiang *et al.*, *Phys. Rev. B* **89**, 214113 (2014).
40. M. Pereiro *et al.*, *Nature Commun.* **5**, 4815 (2014).
41. A. Hierro-Rodriguez *et al.*, *Phys. Rev. B* **95**, 014430 (2017).
42. See Supplemental Material for detailed description, which includes Refs. [43-47].

43. B.-K. Lai *et al.*, Phys. Rev. Lett. **96**, 137602 (2006).
44. I. Kornev, H. Fu and L. Bellaiche, Phys. Rev. Lett. **93**, 196104 (2004).
45. B.-K. Lai, I. A. Kornev, L. Bellaiche and G. J. Salamo, Appl. Phys. Lett. **91**, 152909 (2007).
46. S. K. Streiffer *et al.*, Phys. Rev. Lett. **89**, 067601 (2002).
47. A. Schilling *et al.*, Phys. Rev. B **74**, 024115 (2006).
48. I. Ponomareva, I.I. Naumov, I.A. Kornev, H. Fu and L. Bellaiche, Phys. Rev. B **72**, 140102(R) (2005).
49. Y. Nahas, I. Prokhorenko and L. Bellaiche, Phys. Rev. Lett. **116**, 127601 (2016).
50. C. L. Jia *et al.*, Acta Materialia **82**, 356 (2015).

* Corresponding author.

c.jia@fz-juelich.de; c.jia@mail.xjtu.edu.cn

† Corresponding author.

laurent@uark.edu

Figure captions

FIG. 1. (a) [100] HAADF image of a superlattice film on the STO substrate. The inset shows a magnified part and atomic details across an interface. (b) Vector map of the unit cell dipoles determined from the image displayed in (a), revealing that the dipoles with evident modulus values occur in the PTO layers (yellow areas). Blue half circles denote similar configuration of dipoles. The red frames mark the locations with special dipole configurations, which are magnified and shown in Figs. 2 and 3.

FIG. 2. (a) Magnified map from the part of frame “a” in Fig. 1b, showing a polarization domain with hyperbola shape (pink-green area) and a dipole vortex with a characteristic flow-out swirl (red curved arrows). The red ellipse marks a small vortex, where the in-plane dipole moments are relatively small. (b) Magnified map from the part of frame “b” in Fig. 1b, showing details of dipole wave in the PTO film layer. The small blue circle marks the “bubble” of the dipole wave. (c) Numerically simulated equilibrium dipolar waves in a PTO film under -0.6% compressive strain showing excellent reproduction of the experimental observation in (b).

FIG 3. (a) Magnified map from the part of frame “c” in Fig. 1b, showing a 180° dipole disclination. (b) Numerically simulated metastable disclination in a PTO film under -0.6% compressive strain demonstrating excellent fit to the experimental observation in (a).

FIG. 4. Distinct configurations of dipoles in the first PTO film layer. Between the regular (three) hyperbola domains (pink-green areas) regions show the same polarization direction and include a small central part (small green ellipses) where the dipoles behavior differently from the surroundings.

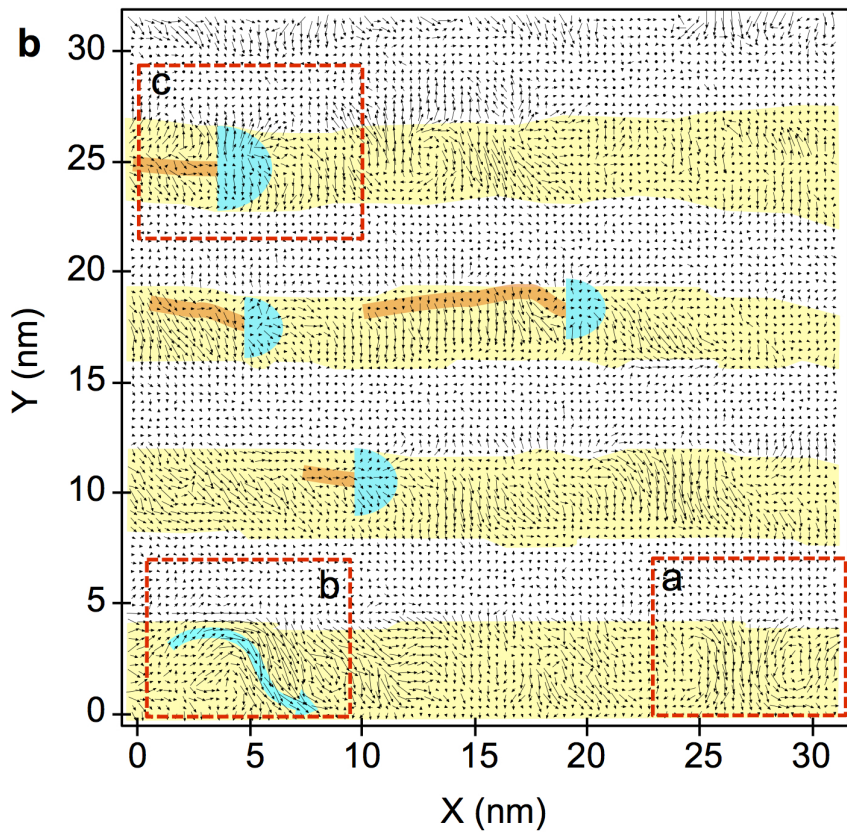
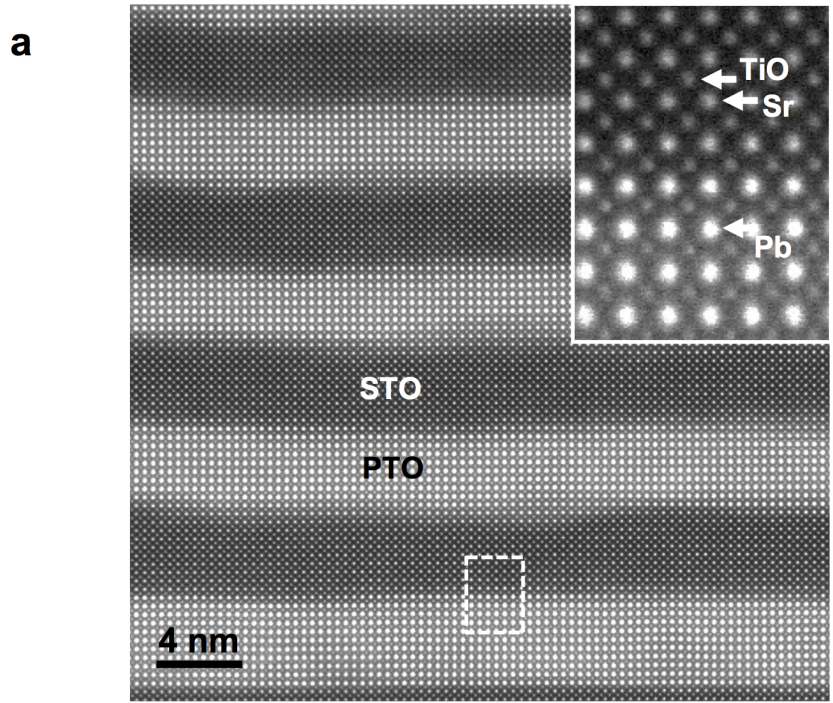


Figure 1

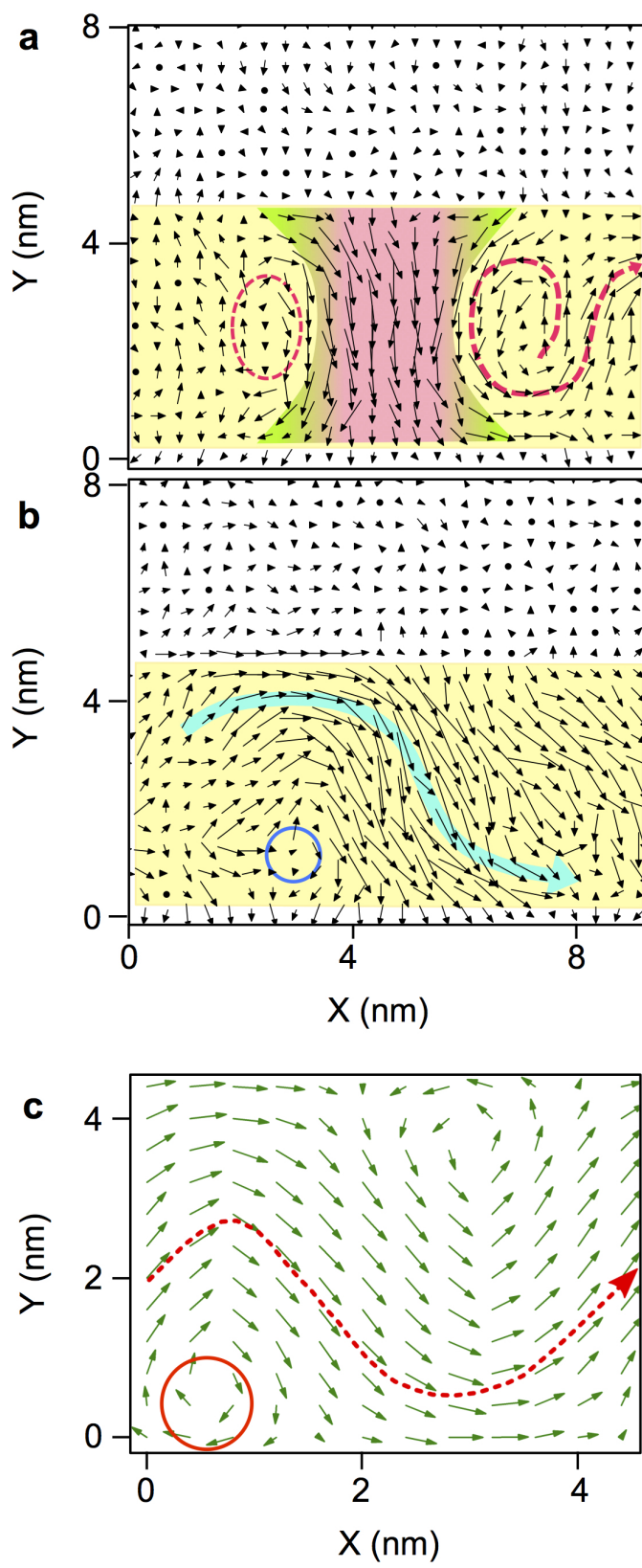


Figure 2

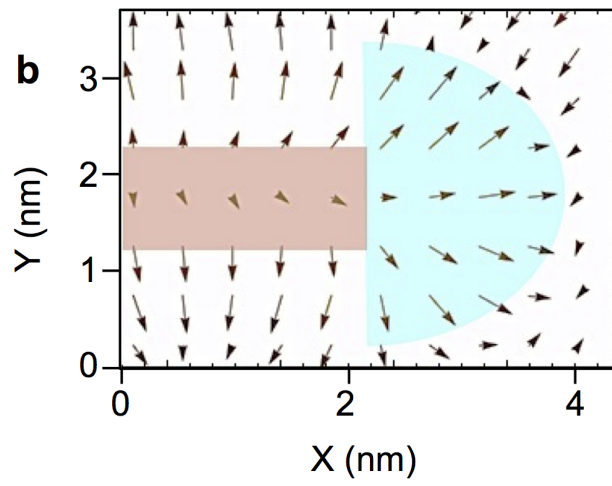
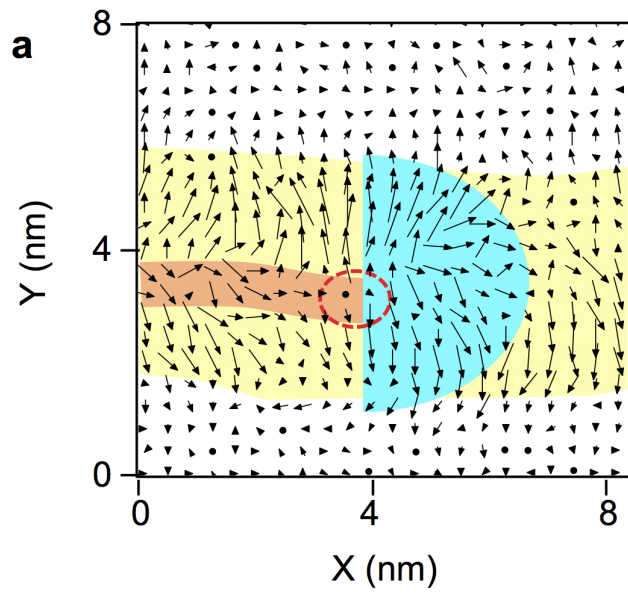


Figure 3

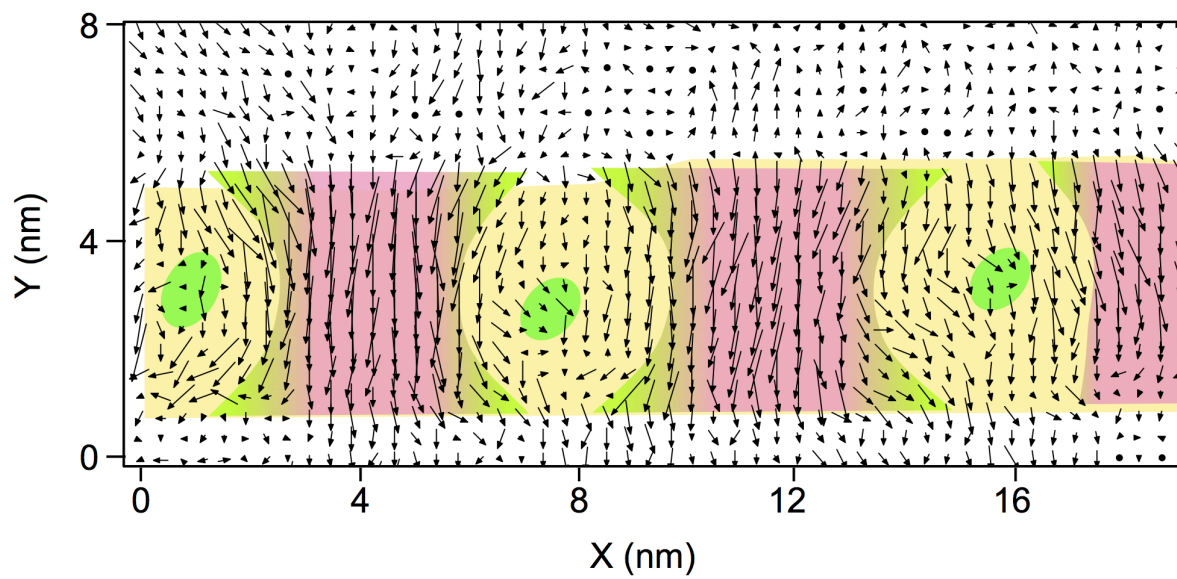


Figure 4